REGULAR ARTICLE

Theoretical studies on N-loss predissociation mechanisms of N₂O⁺ (A $^2\Sigma^+$) in C_s symmetry

Qingyong Meng · Hai-Bo Chang · Ming-Bao Huang ·
Hua Dong

Abstract The N-loss predissociation mechanisms of the A $^2\Sigma^+$ (2 $^2A'$) state of N₂O⁺ to the first and second dissociation limits were studied in the C_s symmetry. The potential energy curves (PECs) and minimum energy crossing points (MECPs) for the C_s states of N₂O⁺ were calculated at the CAS levels. On the basis of our CAS calculation results (CASPT2 energetic results and CASSCF spin orbit couplings), we suggest two processes for N-loss predissociation mechanisms of A $^2\Sigma^+$ (2 $^2A'$) to the first and second limits. The first two steps in the two processes are the same: A $^2\Sigma^+$ passes through the 2 $^2A'/1$ $^4A''$ MECP and then reaches the 1 $^4A''$ (1 $^4\Sigma^-$) PEC. The 2 $^2A'/1$ $^4A''$ MECP has a bent geometry and is slightly higher in energy than the transition state along the 1 $^4A''$ PEC. Our mechanisms are different from the previously suggested mechanisms (via 1 $^4\Pi$).

Keywords N₂O⁺ (A $^2\Sigma^+$) · Predissociation in C_s symmetry · CASPT2 · MECP

1 Introduction

Because the N₂O⁺ ion plays an important role in planetary atmospheres [1], extensive experimental [2–20] and theoretical [21–23] studies on the electronic states and the

Q. Meng · H.-B. Chang · M.-B. Huang (✉) · H. Dong
College of Chemistry and Chemical Engineering,
Graduate University of Chinese Academy of Sciences,
P. O. Box 4588, Beijing 100049, People's Republic of China
e-mail: mbhuang1@gucas.ac.cn

H.-B. Chang
Xi'an Morden Chemistry Research Institute, Xi'an,
Shannxi Province 710065, People's Republic of China

reaction and dissociation mechanisms were reported. Many of the experimental studies were devoted to the photodissociation mechanism of the first excited A state (denoted as A $^2\Sigma^+$ in the literature), and we will mention the experimental studies of Richard-Viard et al. [11] and Xu et al. [17] below. Both the experimental groups observed mainly the N-loss dissociation products: the N (^4S_u) + NO⁺ (X $^1\Sigma^+$) and N (^2D_u) + NO⁺ (X $^1\Sigma^+$) limits, which are the first and second N-loss dissociation limits, respectively (the A $^2\Sigma^+$ state correlates the third N-loss limit of N (^2P_u) + NO⁺ (X $^1\Sigma^+$)).

In 1990, Richard-Viard et al. [11] investigated the predissociation of N₂O⁺ (A $^2\Sigma^+$) using a time of flight (TOF) spectrometer and threshold photoelectron-photoion coincidence (TPEPICO) method within the energy range of 3.31–4.61 eV (from X $^2\Pi$ of N₂O⁺). They found that the predissociation yielded essentially only NO⁺ fragments and both N (^4S_u) + NO⁺ (X $^1\Sigma^+$) and N (^2D_u) + NO⁺ (X $^1\Sigma^+$) limits were reached when energetically accessible. Their suggested mechanism for the N (^4S_u) + NO⁺ (X $^1\Sigma^+$) limit was indirect, the A $^2\Sigma$ state being predissociated by the 1 $^4\Pi$ state via spin–orbit coupling and the 1 $^4\Pi$ state being coupled to the dissociative $^4\Sigma^-$ state leading to the first N-loss limit. They suggested that the second N-loss limit was reached by the spin–orbit coupling of the 1 $^4\Pi$ state with the vibrational continuum of the ground X $^2\Pi$ state. The 1 $^4\Pi$ state was involved in their suggested predissociation mechanisms to the first and second N-loss limits.

In 2004, Xu et al. [17] investigated photodissociation of N₂O⁺ (A $^2\Sigma^+$) using the photofragment excitation (PHOFEX) spectra and TOF mass spectra in the energy region of 3.78–4.51 eV (from X $^2\Pi$ of N₂O⁺), and they observed that at energies below 3.97 eV the dissociation pathway was N (^4S_u) + NO⁺ (X $^1\Sigma^+$) (their channel A), and at

energies above 3.97 eV the dissociation pathway was N (^2D_u) + NO$^+$ (X $^1\Sigma^+$) (their channel B). They [17] suggested the same mechanism for channel A as that of Richard-Viard et al. [11] for the N (^4S_u) + NO$^+$ (X $^1\Sigma^+$) limit (the 1 $^4\Pi$ state being involved). They [17] suggested that the dissociation via channel B was caused by the vibronic coupling between A $^2\Sigma^+$ and X $^2\Pi$. This mechanism (the 1 $^4\Pi$ state is not involved) is different from that (1 $^4\Pi$ was involved) suggested by Richard-Viard et al. [11] for the second N-loss limit.

In 2000, Chambaud et al. [23] reported their theoretical study on photodissociation mechanism of the A $^2\Sigma^+$ state using complete active space self-consistent field (CASSCF) and internally contracted multireference configuration interaction (MRCI) calculations and suggested that A $^2\Sigma^+$ predissociated in bent structures via a spin–orbit coupling with the $^4A''$ component of the $^4\Pi$ state and then transition to $^4\Sigma^-$ for dissociation to the first N-loss (and O-loss) limit via the $^4\Sigma^-$ state. Their predicted mechanism for the predissociation of A $^2\Sigma^+$ to the first N-loss limit could be expressed by the following equation: A $^2\Sigma^+ \rightarrow A$ $^2\Sigma^+/$ $^4A''(1^4\Pi)$ CI (conical intersection) $\rightarrow 1$ $^4\Pi \rightarrow 1$ $^4\Pi/1$ $^4\Sigma^-$ CI $\rightarrow 1$ $^4\Sigma^- \rightarrow$ N (^4S_u) + NO$^+$($X^1\Sigma^+$). This theoretical mechanism is similar to that suggested by Richard-Viard et al. [11] for the first N-loss limit, and it involved the 1 $^4\Pi$ state. The authors did not predict mechanism for predissociation of A $^2\Sigma^+$ to the second N-loss limit in their paper [23]. We note that Chambaud et al. [23] considered the predissociation in bent structures (nonlinear conformation in the C_s symmetry) in their calculations, and we also note that their CASSCF potential energy curves (PECs) did not well converge to the dissociation product limits because their PECs obtained in the single-point energy calculations were not the minimum-energy paths.

The purpose of the present theoretical work is to study N-loss dissociation processes from the A $^2\Sigma^+$ state of N$_2$O$^+$ in bent configuration (in the C_s symmetry) using multiconfiguration second-order perturbation theory (CASPT2) [24, 25] and CASSCF [26] calculations. Based on our predicted mechanisms, we will try to explain the experimental facts in Refs. [11, 17] and examine the suggested mechanisms in the previous experimental [11, 17] and theoretical [23] papers. The CASPT2 method was successfully used in our previous theoretical studies for excited states and dissociation mechanisms of small molecular ions [27–30].

In the previously suggested predissociation mechanisms [11, 17, 23] for the A $^2\Sigma^+$ state of N$_2$O$^+$, the X $^2\Pi$, 1 $^4\Sigma^-$, and 1 $^4\Pi$ states were involved. Since we consider the predissociation mechanisms in the C_s symmetry, we calculated the 1 $^2A'$, 1 $^2A''$, 1 $^4A''$, 2 $^2A'$, 1 $^4A'$, and 2 $^4A''$ states of N$_2$O$^+$, instead of X $^2\Pi$, 1 $^4\Sigma^-$, A $^2\Sigma^+$, and 1 $^4\Pi$. The

calculations performed in the present work included the CASPT2 geometry optimization and CASPT2 N-loss dissociation potential energy curve (PEC) calculations for the six C_s states and the CASSCF minimum energy crossing point (MECP) and spin–orbit coupling calculations for the state/state pairs selected among the six states. The X $^2\Pi$, 1 $^4\Sigma^-$, and 1 $^4A''$ states were already calculated in our previous CASPT2 study for adiabatic and nonadiabatic mechanisms of the N$_2$ (X $^1\Sigma_g^+$) + O$^+$ (^4S_u) reaction, [29] and the 1 $^4A''$ (not 1 $^4\Sigma^-$) state was shown to be important for both the mechanisms.

2 Calculation details

Geometry and atom labeling used for the N$_2$O$^+$ ion in the C_s symmetry are shown in Fig. 1. The CASSCF and CASPT2 calculations were carried out using MOLCAS v7.4 quantum chemistry software [31]. As in our previous CASPT2 study for the N$_2$ + O$^+$ reaction, [29] a large ANO-L basis set, [32–35] N[6s5p4d2f]/O[6s5p4d2f], was used and the full valence active spaces for the N$_2$O$^+$ ion and product species (NO$^+$, NO, N, and N$^+$) were used in the CAS calculations. In all the CASPT2 calculations, the weight values of the CASSCF reference functions in the first-order wave functions were all larger than 0.88. The level shift was not used in our CASPT2 calculations.

The N-loss dissociation PECs were calculated for the C_s states of the N$_2$O$^+$ ion at the CASPT2 level. At a set of fixed R(N$_1$–N$_2$) (see Fig. 1) values ranging from the different starting values (see Sect. 3.2) to 4.0 Å, the CASPT2 partial geometry optimization calculations were performed. The CASPT2 N-loss dissociation PECs for the C_s states were drawn on the basis of the CASPT2 energies at the sets of partially optimized geometries. The N$_2$O$^+$ systems in the different states at the R(N$_1$–N$_2$) value of 4.0 Å are called N-loss asymptote products for the respective states.

For studying nonadiabatic processes, we performed the CASSCF MECP calculations for the state/state pairs selected among the C_s states and then calculated the CASPT2 energies and CASSCF spin orbital coupling
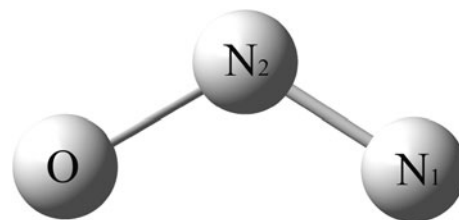

Fig. 1 Atom labelings for the N$_2$O$^+$ ion in the C_s symmetry used in the present work

values at the located MECPs. For the purpose of discussion, we also performed MECP calculations for some $C_{\infty v}$-state/$C_{\infty v}$-state pairs (the CAS calculations for the $C_{\infty v}$ states should be performed in the C_{2v} subgroup of $C_{\infty v}$, see Refs. [28, 29]).

3 Results and discussion

3.1 The C_s states of the N_2O^+ ion

In Table 1 given are the CASPT2 optimized geometries and T_0 values for the $1\,^2A'$, $1\,^2A''$, $2\,^2A'$, $1\,^4A'$, $1\,^4A''$, and $2\,^4A''$ states of the N_2O^+ ion.

The CASPT2 geometry optimization calculations indicate that the $1\,^2A'$, $1\,^2A''$, and $2\,^2A'$ states have the linear equilibrium geometries, and then the $1\,^2A'$ and $1\,^2A''$ states converge to $X\,^2\Pi$ and the $2\,^2A'$ state goes back to $A\,^2\Sigma^+$. The $X\,^2\Pi$ state was calculated in our previous CASPT2 study, [29] but the results were not reported in Ref. [29]. By comparing the calculated and experimental geometries of the $X\,^2\Pi$ and $A\,^2\Sigma^+$ states, we note that the N_2–O bond length values in the CASPT2 geometries of the two states are close to the experimental values [5] while the N_1–N_2 bond length values in the CASPT2 geometries of the two states are (around 0.013 Å) smaller than the experimental values [5]. The same tendencies are found in the MRCI geometries [23] (see Table 1) of the two states. The CASPT2 T_0 value (3.38 eV) for the $A\,^2\Sigma^+$ state is 0.11 eV smaller than the experimental value [3, 18] (the MRCI value is slightly larger than the experimental value).

Along the CASPT2 $1\,^4A''$ energy profile (adiabatic path) of the N_2 ($X\,^1\Sigma_g^+$) + O^+ (^4S_u) → NO^+ ($X\,^1\Sigma^+$) + N (^4S_u) reaction reported in Ref. [29], there are two minima and a transition state (TS) in between. In Table 1 of the present paper, we list the CASPT2 calculation results for the global minimum (denoted as $1\,^4A''$) and the transition state (denoted as $1\,^4A''$ (TS)). The other minimum is a local minimum along the O-loss dissociation path. The N_1N_2O angle values in the CASPT2 geometries of $1\,^4A''$ and $1\,^4A''$ (TS) are 106.0° and 115.0°, respectively, and the $1\,^4A''$ geometry has a long N_1–N_2 bond of 2.724 Å.

The CASPT2 calculations predict a linear geometry for the $1\,^4A'$ state and a bent geometry with an N_1N_2O angle of 111.4° for the $2\,^4A''$ state. Since the CASPT2 T_0 value (6.51 eV) for $2\,^4A''$ is very high, we will not perform more calculations for this state.

3.2 N-loss dissociation potential energy curves

The CASPT2 N-loss dissociation PECs of the $1\,^2A'$, $1\,^2A''$, $2\,^2A'$, $1\,^4A''$, and $1\,^4A'$ states are given in Fig. 2, and they were obtained based on the CASPT2 partial geometry optimization calculations. Since too high in energy, the $2\,^4A''$ N-loss PEC was not calculated. The starting $R(N_1$–$N_2)$ values for the $1\,^2A'$, $1\,^2A''$, and $2\,^2A'$ PECs were the N_1–N_2 bond length values (1.140, 1.140, and 1.127 Å, respectively) in the CASPT2 geometries of the three states. The starting $R(N_1$–$N_2)$ value for the $1\,^4A''$ PEC was the N_1–N_2 bond length value of 1.179 Å in the CASPT2 geometry of $1\,^4A''$ (TS). The starting $R(N_1$–$N_2)$ value for the $1\,^4A'$ PEC was 1.2 Å.

Table 1 CASPT2 optimized geometries and adiabatic relative energies (T_0, in eV) for the $1\,^2A'$, $1\,^2A''$, $2\,^2A'$, $1\,^4A'$, $1\,^4A''$, and $2\,^4A''$ states of the N_2O^+ ion (bond lengths are given in Å and bond angles in degrees; for notations, see Fig. 1)

State	Geometry [$R(N_1$–$N_2)$, $R(N_2$–O), ∠N_1N_2O]			T_0		
	CASPT2	MRCI[a]	Expt.[b]	CASPT2[c]	MRCI[a]	Expt.[d]
$X\,^2\Pi$ ($1\,^2A'$, $1\,^2A''$)	1.140, 1.188, 180.0	1.137, 1.192	1.154, 1.185	0.0 (0.0)	0.0	0.0
$A\,^2\Sigma^+$ ($2\,^2A'$)	1.127, 1.145, 180.0	1.123, 1.138	1.140, 1.141	3.29 (3.38)	3.55	3.49[e], 3.50[f]
$1\,^4A''$[g]	2.724, 1.064, 106.0			1.54 (1.47)		
$1\,^4A''$ (TS)[g]	1.179, 1.441, 115.0			3.10 (2.99)		
$1\,^4A'$	1.476, 1.150, 180.0			4.33 (4.27)		
$2\,^4A''$	1.435, 1.282, 111.4			6.51 (6.39)		

[a] Ref. [23]

[b] Ref. [5]

[c] Values in parentheses are the T_0 values with CASSCF ZPE corrections

[d] Experimental T_0 values are evaluated using the experimental adiabatic ionization energy data

[e] Ref. [3, 18]

[f] Ref. [5, 15]

[g] Along the CASPT2 $1\,^4A''$ energy profile for the N_2 + O^+ → NO^+ + N reaction reported in Ref. [29], there are two minima and a transition state in between. In this table the CASPT2 results for the global minimum ($1\,^4A''$) and the transition state ($1\,^4A''$ (TS)) are listed (the local minimum is along the O-loss dissociation path)

According to the group theory, the $1\,^2A'$, $1\,^2A''$, $2\,^2A'$, $1\,^4A''$, and $1\,^4A'$ states of the N_2O^+ ion correlate with NO^+ $(X\,^1\Sigma^+) + N\ (^2D_u)$, NO^+ $(X\,^1\Sigma^+) + N\ (^2D_u)$, NO^+ $(X\,^1\Sigma^+) + N\ (^2P_u)$, NO^+ $(X\,^1\Sigma^+) + N\ (^4S_u)$, and NO $(X\,^2\Pi) + N^+\ (^3P_g)$, which are the second, second, third, first, and fourth N-loss dissociation limits, respectively. The sum energies of these product groups relative to the $X\,^2\Pi$ reactant (abbreviated to "energies for the N-loss limits") were obtained in the CASPT2 calculations (including the geometry optimization calculations for the NO^+ and NO and energy calculations for $N\ (^4S_u)$, $N\ (^2D_u)$, $N\ (^2P_u)$, and $N^+\ (^3P_g)$), and the CASPT2 energies for the first, second, third, and fourth N-loss limits are 1.68, 4.08, 5.24, and 7.01 eV, respectively. The CASPT2 energies of the asymptote products along the $1\,^2A'$, $1\,^2A''$, $2\,^2A'$, $1\,^4A''$, and $1\,^4A'$ PECs relative to the $X\,^2\Pi$ reactant (abbreviated to "CASPT2 energies of the asymptote products") are 4.04, 4.04, 5.20, 1.63, and 7.10 eV, which are very close to the CASPT2 energies for the second, second, third, first, and fourth N-loss limits, respectively. Therefore, the CASPT2 energetic results (also the O–N_2 fragmental geometries and charge distributions in the asymptote products) confirm that the $1\,^2A'$, $1\,^2A''$, $2\,^2A'$, $1\,^4A''$, and $1\,^4A'$ states of the N_2O^+ ion correlate with NO^+ $(X\,^1\Sigma^+) + N\ (^2D_u)$, NO^+ $(X\,^1\Sigma^+) + N\ (^2D_u)$, NO^+ $(X\,^1\Sigma^+) + N\ (^2P_u)$, NO^+ $(X\,^1\Sigma^+) + N\ (^4S_u)$, and NO $(X\,^2\Pi) + N^+\ (^3P_g)$, respectively. However, our CASPT2 energies of 1.68, 4.08, 5.24, and 7.01 eV for the first, second, third, and fourth N-loss limits are larger than the experimental energies [7, 12, 18] of 1.30, 3.68, 4.88, and 6.56 eV, respectively, and the discrepancy between the

CASPT2 and experimental energies is around 0.4 eV for each of the limits (the CASPT2 energies with CASSCF zero-point energy corrections are still 0.19–0.25 eV larger than the experimental energies). In our previous CASPT2 studies [27–30] for dissociation of other molecular ions, the discrepancies between the CASPT2 and experimental energies for the dissociation limits were not large (smaller than 0.18 eV), and we do not know the reasons for the large discrepancies of around 0.4 eV in this case.

The $1\,^2A'$ and $1\,^2A''$ PECs were not given in Ref. [29], but the N_1N_2O angle values at some $R(N_1–N_2)$ values along the CASPT2 $1\,^2A'$ and $1\,^2A''$ PECs were given in Table 2 of Ref. [29]. As shown in that table, the $1\,^2A'$ and $1\,^2A''$ partially optimized geometries at the $R(N_1–N_2)$ values between 1.8 and 2.5 Å are bent with different N_1N_2O angle values. The CASPT2 PECs of the two states do not coincide in that region (see Fig. 2). The $1\,^4A''$ PEC was already calculated in our previous study [29]. The N_1N_2O angle values at the $R(N_1–N_2)$ values smaller than 2.2 Å along the N-loss PEC of the $1\,^4A''$ state are smaller than 120° (see Table 2 of Ref. [29]). The $1\,^4\Sigma^-$ PEC was also calculated in our previous study [29]. As shown in Fig. 3 of Ref. [29], the $1\,^4\Sigma^-$ PEC lies above the $1\,^4A''$ PEC and the $1\,^4\Sigma^-$ energy greatly increases when the $R(N_1–N_2)$ value becomes small. The present calculations indicate that the partially optimized geometries along the CASPT2 PECs of the $2\,^2A'$ and $1\,^4A'$ states are linear, and therefore the $2\,^2A'$ PEC in Fig. 2 is just the $A\,^2\Sigma^+$ PEC. There is a transition state (denoted as TS ($2\,^2A'$)) at a $R(N_1–N_2)$ value of around 1.6 Å along the CASPT2 PEC of the $2\,^2A'$ ($A\,^2\Sigma^+$) state. The CASPT2 geometry optimization calculations predict

Table 2 Locations (geometries) of the minimum energy crossing points (MECPs) for selected C_s-state/C_s-state pairs predicted by the CASSCF calculations, together with the CASSCF spin–orbit coupling values (in cm^{-1}) and CASPT2 state/state energies ($\Delta E/\Delta E$ in eV, relative to $X\,^2\Pi$) at the CASSCF MECPs (bond lengths are given in Å and bond angles in degrees)

State/state	CASSCF MECP geometry			Spin–orbit coupling	CASPT2 $\Delta E/\Delta E$[a]
	$R(N_1–N_2)$	$R(N_2–O)$	$\angle N_1N_2O$		
C_s symmetry					
$2\,^2A'/1\,^4A''$	1.194	1.189	151.0	53.8	3.82/3.66 (3.74)
	[1.169][b]	[1.172]	[155.0]		
$2\,^2A'/1\,^4A'$ (1)	1.536	1.155	139.0	4.8	4.15/4.36 (4.26)
$2\,^2A'/1\,^4A'$ (2)	1.910	1.127	180.0	0.0	5.20/5.00 (5.10)
$1\,^4A''/1\,^2A'$	1.449	1.138	127.0	58.5	2.27/2.18 (2.22)
$1\,^4A''/1\,^2A''$	1.488	1.133	128.7	70.9	2.26/2.19 (2.22)
	[1.482][b]	[1.111]	[130.0]		
$C_{\infty v}$ symmetry					
$A\,^2\Sigma^+/1\,^4\Pi$ (1)	1.303	1.168	180.0	2.3	4.45/4.32 (4.38)
$A\,^2\Sigma^+/1\,^4\Pi$ (2)	1.910	1.127	180.0	0.0	5.20/5.00 (5.10)

The results for the $A\,^2\Sigma^+/1\,^4\Pi$ MECPs calculated in $C_{\infty v}$ symmetry are also listed

[a] Values in parentheses are the averages

[b] Values in square brackets are the geometric of "energetically lowest crossings" predicted by the previous MRCI calculations (Ref. [23])
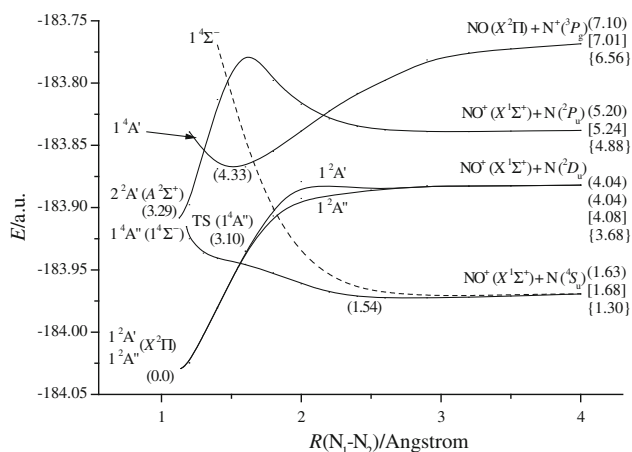
Fig. 2 CASPT2 potential energy curves (PECs) for N-loss dissociation from the $1~^2A'$, $1~^2A''$, $2~^2A'$, $1~^4A'$, and $1~^4A''$ states of the N_2O^+ ion. Values in parentheses are the CASPT2 energies (in eV) of the reactants and asymptote products relative to the $X~^2\Pi$ reactant, and values in square brackets are the CASPT2 sum energies (in eV) of the product groups relative to the $X~^2\Pi$ reactant (values in braces are the experimental sum energies of the product group relative to $X~^2\Pi$). The $1~^4\Sigma^-$ PEC calculated in the $C_{\infty v}$ symmetry is also shown

that TS ($2~^2A'$) is about 6.60 eV higher in energy than the $X~^2\Pi$ reactant and it has a linear geometry ($R(N_1–N_2) =$ 1.610 Å, $R(N_2–O) = 1.110$ Å, and $\angle N_1N_2O = 180.0°$).

In Fig. 2, the $1~^4A''$ PEC crosses the $1~^2A'$ and $1~^2A''$ PECs, and $1~^4A'$ PEC crosses the $2~^2A'$ PEC twice. In Fig. 2, the starting points of the $2~^2A'$ and $1~^4A''$ PECs are very close, but the two PECs will not cross since the stating point of the $2~^2A'$ PEC represents a minimum while the starting point of the $1~^4A''$ PEC represents a transition state.

3.3 Predissociation mechanisms of the $A~^2\Sigma^+$ ($2~^2A'$) state

Our prediction of the predissociation mechanisms is mainly based on the MECP calculations performed in the C_s symmetry for the C_s state pairs.

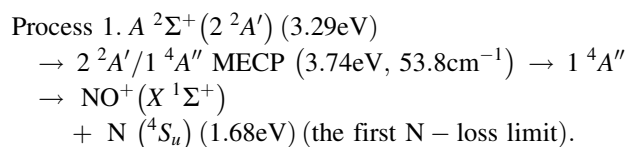#### 3.3.1 MECP calculations for the C_s states

We consider the MECPs for the $2~^2A'/1~^4A''$ and $2~^2A'/1~^4A'$ state pairs, and the $R(N_1–N_2)$ values at the two MECPs should be larger than the value in the $2~^2A'$ ($A~^2\Sigma^+$) geometry since we are considering the N-loss dissociation. The MECPs for the $1~^4A''/1~^2A'$ and $1~^4A''/1~^2A''$ state pairs are also considered, and the $R(N_1–N_2)$ values at the two MECPs should be larger than the value in the $1~^4A''$ (TS) geometry.

In Table 2 listed are the geometries of the CASSCF MECPs for the four state pairs in C_s symmetry, together with the CASSCF spin–orbit coupling values and CASPT2

state/state energies (relative to $X~^2\Pi$) calculated at the CASSCF MECP geometries. We located the $2~^2A'/1~^4A''$ MECP though the $2~^2A'$ and $1~^4A''$ PECs in Fig. 2 do not cross. We located two MECPs for the $2~^2A'/1~^4A'$ state pair (denoted as "$2~^2A'/1~^4A'$ (1) MECP" and "$2~^2A'/1~^4A'$ (2) MECP"). The $1~^4A''/1~^2A'$ and $1~^4A''/1~^2A''$ MECPs were already calculated in our previous study [29]. At each of the located MECPs, the CASSCF energy difference between the two states in the pair is smaller than 0.01 eV and the CASPT2 energy difference is smaller than 0.21 eV (we will use the average of the CASPT2 energies in discussion). The N_1N_2O angle values in the geometries of the $2~^2A'/1~^4A''$, $2~^2A'/1~^4A'$ (1), $1~^4A''/1~^2A'$, and $1~^4A''/1~^2A''$ MECPs are 151.0°, 139.0°, 127.0°, and 128.7°, respectively, and the angle value in the geometry of the $2~^2A'/1~^4A'$ (2) MECP is 180°. The CASSCF spin–orbit coupling values at the $2~^2A'/1~^4A''$, $1~^4A''/1~^2A'$, and $1~^4A''/1~^2A''$ MECPs are larger than 50 cm^{-1}, while the values at the $2~^2A'/1~^4A'$ (1) and $2~^2A'/1~^4A'$ (2) MECPs are very small or zero. Chambaud et al. [23] calculated "the energetically lowest crossings" (MECP) for the $2~^2A'/1~^4A''$ and $1~^4A''/1~^2A''$ state pairs at the MRCI level, and the geometries (listed in Table 2) of their two MECPs are quite close to the geometries of our MECPs, respectively.

3.3.2 Predicted N-loss predissociation mechanisms of the $A~^2\Sigma^+$ ($2~^2A'$) state in the C_s symmetry

On the basis of the above-reported calculation results (PECs, for the C_s states, including the N-loss PECs and energies and spin–orbit couplings at the MECPs), the mechanism of the N-loss predissociation from $A~^2\Sigma^+$ ($2~^2A'$) to the first limit is predicted to follow the following process:
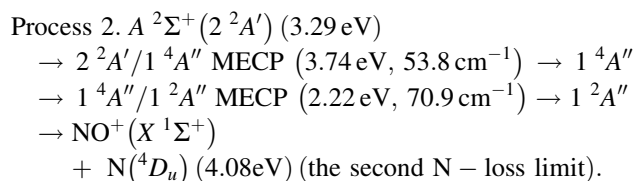
Process 1. $A~^2\Sigma^+\left(2~^2A'\right)$ (3.29eV)
  $\rightarrow 2~^2A'/1~^4A''$ MECP $\left(3.74\text{eV},~53.8\text{cm}^{-1}\right) \rightarrow 1~^4A''$
  $\rightarrow NO^+\left(X~^1\Sigma^+\right)$
    $+ N\left(^4S_u\right)$ (1.68eV) (the first N $-$ loss limit).

In parentheses are the CASPT2 relative energy values to $X~^2\Pi$ and the CASSCF spin–orbit coupling value at the MECP.

Since the $2~^2A'/1~^4A'$ (1) and $2~^2A'/1~^4A'$ (2) MECPs are higher in energy than the $2~^2A'/1~^4A''$ MECP and have very small spin orbit couplings (4.8 and 0.0 cm^{-1}), the predissociation process of the $A~^2\Sigma^+$ ($2~^2A'$) state will pass the $2~^2A'/1~^4A''$ MECP (as the first step) and will not pass the $2~^2A'/1~^4A'$ (1) or $2~^2A'/1~^4A'$ (2) MECP.

In the second step of process 1, the N_2O^+ system is considered to go from the $2~^2A'/1~^4A''$ MECP to the $1~^4A''$ PEC. The average CASPT2 energy (3.74 eV) at the $2~^2A'/1~^4A''$ MECP is higher than the CASPT2 energies of $A~^2\Sigma^+$

$(2\ ^2A')$ (3.29 eV) and TS $(1\ ^4A'')$ (3.10 eV) and the (CASSCF) $R(N_1-N_2)$ value (1.194 Å) in the $2\ ^2A'/1\ ^4A''$ MECP is lightly larger than the (CASPT2) $R(N_1-N_2)$ values in the geometries of $A\ ^2\Sigma^+$ $(2\ ^2A')$ (1.127 Å) and TS $(1\ ^4A'')$ (1.179 Å). For exploring the path from the $2\ ^2A'/1\ ^4A''$ MECP to the $1\ ^4A''$ PEC, we carried out the following testing calculations. We performed the CASPT2 single-point energy calculations in the $1\ ^4A''$ PES at the ten uniformly interpolated geometries between the $2\ ^2A'/1\ ^4A''$ MECP (CASSCF) geometry $(R(N_1-N_2) = 1.194$ Å, $R(N_2-O) = 1.189$ Å, and $\angle N_1N_2O = 151.0°)$ and the TS $(1\ ^4A'')$ (CASPT2) geometry $(R(N_1-N_2) = 1.179$ Å, $R(N_2-O) = 1.441$ Å, and $\angle N_1N_2O = 115.0°)$. We find that the CASPT2 energy along this "path" monotonously decreases from 3.66 eV (the CASPT2 energy of $1\ ^4A''$ at the $2\ ^2A'/1\ ^4A''$ MECP) to 3.10 eV (the CASPT2 energy of TS $(1\ ^4A'')$), which indicates that this is an energetically feasible path. This fact implies that the N_2O^+ system can go from the $2\ ^2A'/1\ ^4A''$ MECP to the $1\ ^4A''$ PEC, though we do not know the optimal path in the $1\ ^4A''$ PES from the $2\ ^2A'/1\ ^4A''$ MECP to a special point along the $1\ ^4A''$ PEC.

The mechanism of the N-loss predissociation from $A\ ^2\Sigma^+$ $(2\ ^2A')$ to the second limit is predicted to follow the following process:

Process 2. $A\ ^2\Sigma^+\left(2\ ^2A'\right)$ (3.29 eV)
$\rightarrow 2\ ^2A'/1\ ^4A''$ MECP $\left(3.74\,\text{eV},\ 53.8\,\text{cm}^{-1}\right) \rightarrow 1\ ^4A''$
$\rightarrow 1\ ^4A''/1\ ^2A''$ MECP $\left(2.22\,\text{eV},\ 70.9\,\text{cm}^{-1}\right) \rightarrow 1\ ^2A''$
$\rightarrow NO^+\left(X\ ^1\Sigma^+\right)$
$\quad + N\left(^4D_u\right)$ (4.08 eV) (the second N − loss limit).

The first two steps in process 2 are the same as in process 1. In the third step of process 2, we have considered the $1\ ^4A''/1\ ^2A''$ MECP (rather than the $1\ ^4A''/1\ ^2A'$ MECP), because the spin orbit coupling value at the $1\ ^4A''/1\ ^2A''$ MECP is larger than that at the $1\ ^4A''/1\ ^2A'$ MECP.

The maximum CASPT2 relative energy values along processes 1 and 2 are 3.74 and 4.08 eV, respectively, which can be considered as the needed energies (from $X\ ^2\Pi$) for N-loss predissociation of $A\ ^2\Sigma^+$ to the first and second limits, respectively.

3.4 Discussion on the previously suggested mechanisms for N-loss predissociation of the $A\ ^2\Sigma^+$ state

For the N-loss predissociation from $A\ ^2\Sigma^+$ to the first limit, the first steps of the suggested mechanisms by the previous experimental studies [11, 17] were considered to proceed via the interaction of the $A\ ^2\Sigma^+$ state with the $1\ ^4\Pi$ state (or a component of $1\ ^4\Pi$). In the suggested mechanism by Richard-Viard et al. [11] for the N-loss predissociation

from $A\ ^2\Sigma^+$ to the second limit, the first step was also considered to proceed via the interaction of the $A\ ^2\Sigma^+$ state with $1\ ^4\Pi$. For discussing these suggested mechanisms, we calculated the $A\ ^2\Sigma^+/1\ ^4\Pi$ MECP in the $C_{\infty v}$ symmetry.

We located two MECPs for the $A\ ^2\Sigma^+/1\ ^4\Pi$ state pair (denoted as "$A\ ^2\Sigma^+/1\ ^4\Pi$ (1) MECP" and "$A\ ^2\Sigma^+/1\ ^4\Pi$ (2) MECP", see Table 2). At the two $A\ ^2\Sigma^+/1\ ^4\Pi$ MECPs, the CASSCF spin orbit coupling values are very small (2.3 and $0.0\,\text{cm}^{-1}$) and the CASPT2 average energy values are larger than those at all the MECPs calculated in the C_s symmetry (see Table 2). Therefore, our calculations do not support the mechanisms for the N-loss predissociation from $A\ ^2\Sigma^+$ to the first [11, 17] and second [17] limits suggested in the experimental papers, since the first steps of these suggested mechanisms were considered to proceed via the $1\ ^4\Pi$ state.
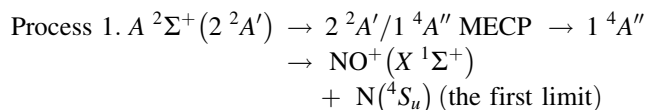
In the experimental study of Xu et al. [17], the N-loss predissociation from $A\ ^2\Sigma^+$ to the second limit was suggested to proceed via the vibronic coupling between $A\ ^2\Sigma^+$ and $X\ ^2\Pi$. We would think that the vibronic coupling between $A\ ^2\Sigma^+$ and $X\ ^2\Pi$ might be weak, since the energy gaps between the $A\ ^2\Sigma^+$ $(2\ ^2A')$ and $X\ ^2\Pi$ $(1\ ^2A'$ and $1\ ^2A'')$ PECs are large in Fig. 2.

In the previous theoretical study, [23] the predicted mechanism for the N-loss predissociation from $A\ ^2\Sigma^+$ to the first limit involved the $1\ ^4\Pi$ state ($^4A''$ component). In the first steps of our predicted mechanisms for the N-loss predissociation from $A\ ^2\Sigma^+$ to the first and second limits (see processes 1 and 2), the involved interaction is that between $2\ ^2A'$ $(A\ ^2\Sigma^+)$ and $1\ ^4A''$ $(1\ ^4\Sigma^-)$ (not that between $A\ ^2\Sigma^+$ and $1\ ^4\Pi$). Actually, Chambaud et al. [23] already calculated the $2\ ^2A'/1\ ^4A''$ MECP at the MRCI level, and we have listed the geometry in Table 2. We think that their located $2\ ^2A'/1\ ^4A''$ MECP [23] is just our $2\ ^2A'/1\ ^4A''$ MECP (the geometry of their MECP is quite close to that of our MECP, though their MRCI relative energy value is about 0.4 eV larger than our CASPT2//CASSCF average relative energy value). In the C_s symmetry, the $1\ ^4A''$ potential energy surface has character of $1\ ^4\Sigma^-$ in some regions and has character of the $^4A''$ component of $1\ ^4\Pi$ in other regions. However, Chambaud et al. [23] considered that the N_2O^+ system would go to $1\ ^4\Pi$ from the $2\ ^2A'/1\ ^4A''$ MECP (back to the linear dissociation path) and then to $^4\Sigma^-$ for dissociating to the first N-loss limit. We consider that in the next step of the predissociation the N_2O^+ system reaches the dissociative $1\ ^4A''$ $(1\ ^4\Sigma^-)$ state (at the TS $(1\ ^4A'')$).
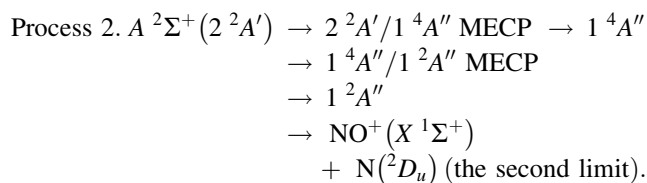
4 Conclusions

The main purpose of the present work is to study the N-loss predissociation mechanisms of the $A\ ^2\Sigma^+$ $(2\ ^2A')$ state of the N_2O^+ ion to the first and second limits in C_s symmetry. We calculated the CASPT2 geometries and T_0 values for

the $1\ ^2A'$, $1\ ^2A''$, $2\ ^2A'$, $1\ ^4A''$, $1\ ^4A'$, and $2\ ^4A''$ states (the $1\ ^2A'$ and $1\ ^2A''$ states converge to $X\ ^2\Pi$ and the $2\ ^2A'$ state to $A\ ^2\Sigma^+$). We calculated the CASPT2 N-loss dissociation PECs for the $1\ ^2A'$, $1\ ^2A''$, $2\ ^2A'$, $1\ ^4A''$, and $1\ ^4A'$ states and performed the MECP calculations in C_s symmetry (including the CASSCF MECP geometries and the CAS-PT2//CASSCF energies and CASSCF spin orbit couplings at the MECPs). On the basis of our CAS calculation results (CASPT2 energetic results and CASSCF spin orbit couplings), we suggest the following two processes for the N-loss predissociation mechanisms of $A\ ^2\Sigma^+$ ($2\ ^2A'$) to the first and second limits:

Process 1. $A\ ^2\Sigma^+ \left(2\ ^2A'\right) \rightarrow 2\ ^2A'/1\ ^4A''$ MECP $\rightarrow 1\ ^4A''$
$$\rightarrow \mathrm{NO}^+\left(X\ ^1\Sigma^+\right)$$
$$+\ \mathrm{N}\left(^4S_u\right) \text{(the first limit)}$$

and

Process 2. $A\ ^2\Sigma^+ \left(2\ ^2A'\right) \rightarrow 2\ ^2A'/1\ ^4A''$ MECP $\rightarrow 1\ ^4A''$
$$\rightarrow 1\ ^4A''/1\ ^2A''\ \text{MECP}$$
$$\rightarrow 1\ ^2A''$$
$$\rightarrow \mathrm{NO}^+\left(X\ ^1\Sigma^+\right)$$
$$+\ \mathrm{N}\left(^2D_u\right) \text{(the second limit)}.$$

The $2\ ^2A'/1\ ^4A''$ MECP is involved in the first steps of both the processes, and it has a bent geometry. The CASPT2 energy (3.74 eV) at the $2\ ^2A'/1\ ^4A''$ MECP is slightly higher than the CASPT2 energies of the stationary points in the $2\ ^2A'$ and $1\ ^4A''$ potential energy surfaces, i.e. $A\ ^2\Sigma^+$ (3.29 eV) and TS ($1\ ^4A''$) (3.10 eV). The N_1–N_2 bond length value in the $2\ ^2A'/1\ ^4A''$ MECP is close to those in the geometries of the two stationary points. In the second steps of both the two processes, the N_2O^+ system goes along the $1\ ^4A''$ PEC. The N_1N_2O angle values at small $R(N_1$–$N_2)$ values (<2.2 Å) along the $1\ ^4A''$ PEC are around $120°$, and the $1\ ^4A''$ PEC coincides with the $1\ ^4\Sigma^-$ PEC at large $R(N_1$–$N_2)$ values (>2.2 Å).

The previous experimental [11, 17] and theoretical [23] studies considered that N_2O^+ ($A\ ^2\Sigma^+$) would go to the $1\ ^4\Pi$ state (via bent component) and then to $1\ ^4\Sigma^-$ in the predissociation to the first N-loss limit. In the present study, we consider that N_2O^+ ($A\ ^2\Sigma^+/2\ ^2A'$) goes from the $2\ ^2A'/1\ ^4A''$ MECP to the dissociating $1\ ^4A''$ ($1\ ^4\Sigma^-$) state as the second step.

References

1. Berkowitz J, Groenveld KO (1983) Molecular ions: geometric and electronic structures. Plenum, New York

2. Dunbar RC (1971) J Am Chem Soc 93:4345
3. Orth RG, Dunbar RC (1977) J Chem Phys 66:1616
4. Hollas JM, Sutherley TA (1973) Chem Phys Lett 21:167
5. Callomon JH, Creutzberg F (1974) Phil Trans R Soc A 277:157
6. Frey R, Gotchev B, Peatman WB, Pollak H, Schlag EW (1978) Chem Phys Lett 54:411
7. Nenner I, Guyon PM, Baer T, Govers TR (1980) J Chem Phys 72:6587
8. Dehmer PM, Dehmer JL, Chupka WA (1980) J Chem Phys 73:126
9. Ibuki T, Sugita N (1984) J Chem Phys 80:4625
10. Lermé J, Abed S, Larzillière M, Holt RA, Carré M (1986) J Chem Phys 84:2167
11. Richard-Viard M, Atabek O, Dutuit O, Guyon PM (1990) J Chem Phys 93:8881
12. Chen S-Y, Ma C-I, Hansond DM, Lee K, Kim DY (1998) J Electron Spectros Relat Phenom 93:61
13. Lebech M, Houver JC, Dowek D, Lucchese RR (2002) J Chem Phys 117:9248
14. Lebech M, Houver JC, Dowek D, Lucchese RR (2004) J Chem Phys 120:8226
15. Chen W, Liu J, Ng CY (2003) J Phys Chem A 107:8086
16. Xu H, Guo Y, Li Q, Liu S, Ma X, Liang J, Li H (2003) J Chem Phys 119:11609
17. Xu H, Guo Y, Li Q, Shi Q, Liu S, Ma X (2004) J Chem Phys 121:3069
18. Céolin D, Travnikova O, Bao Z, Piancastelli MN, Tanaka T, Hoshino M, Kato H, Tanaka H, Harries JR, Tamenori Y, Prümper C, Lischke T, Liu X-J, Ueda K (2008) J Chem Phys 128:024306
19. Imamura T, Imajo T, Koyano I (1995) J Phys Chem 99:15465
20. Hamberg M, Geppert WD, Rosén S, Hellberg F, Ehlerding A, Zhaunerchyk V, Kaminska M, Thomas RD, Af ugglas M, Källberg A, Simonsson A, Paal A, Larsson M (2005) Phys Chem Chem Phys 7:1664
21. Beswick JA, Horani M (1981) Chem Phys Lett 78:4
22. Köppel H, Cederbaum LS, Domcke W (1982) Chem Phys 69:175
23. Chambaud G, Gritli H, Rosmus P, Werner H-J, Knowles PJ (2000) Mol Phys 98:1793
24. Andersson K, Malmqvist P-Å, Roos BO (1995) In: Yarkony DR (ed) Modern electronic structure theory, part 1. World Scientific, Singapore, p 55
25. Andersson K, Roos BO (1993) Int J Quantum Chem 45:591
26. Roos BO (1987) In: Lawley KP (ed) Advances in chemical physics. Wiley, New York, p 399
27. Chang H-B, Huang M-B (2009) Chem Phys Chem 10:582
28. Meng Q, Huang M-B, Chang H-B (2009) J Phys Chem A 113:12825
29. Chang H-B, Meng Q, Huang M-B, Dong H (2010) Mol Phys 108:2137
30. Meng Q, Huang M-B (2011) J Comput Chem 32:142
31. Karlström G, Lindh R, Malmqvist P-Å, Roos BO, Ryde U, Veryazov V, Widmark P-O, Cossi M, Schimmelpfennig B, Neogrady P, Seijo L (2003) Comput Mat Sci 28:222
32. Almlof J, Taylor PR (1987) J Chem Phys 86:4070
33. Pierloot K, Dumez B, Widmark P-O, Roos BO (1995) Theor Chem Acc 90:87
34. Widmark P-O, Malmqvist P-Å, Roos BO (1990) Theor Chem Acc 77:291
35. Widmark P-O, Persson BJ, Roos BO (1991) Theor Chem Acc 79:419